# A canonical chaperone and a heat-resistant obscure (Hero) protein mediate similar conformational modulation and aggregation suppression of TDP-43

Andy Y.W. Lam[1,2], Kotaro Tsuboyama[1,3], Hisashi Tadakuma[1,4], Yukihide Tomari[1,2,*]

1. Institute for Quantitative Biosciences, The University of Tokyo, Bunkyo-ku, Tokyo 113-0032, Japan.
2. Department of Computational Biology and Medical Sciences, Graduate School of Frontier Sciences, The University of Tokyo, Bunkyo-ku, Tokyo 113-0032, Japan
3. Department of Pharmacology, Northwestern University, Chicago, IL 60611, USA
4. School of Life Science and Technology, ShanghaiTech University, Shanghai 201210, People's Republic of China

*Correspondence: tomari@iqb.u-tokyo.ac.jp

**Abstract**

Misfolding and aggregation of proteins are characteristic features in the progression of neurodegenerative diseases. While molecular chaperones are well-known suppressors of these aberrant events, we recently reported that a widespread family of heat-resistant obscure (Hero) proteins may also play a similar role. However, it is unclear how such electrostatically charged intrinsically disordered proteins protect client proteins from denaturation and aggregation. Here we utilize single-molecule FRET to monitor the conformations of an aggregation-prone protein, TDP-43. While we observed high conformational heterogeneity of wild-type TDP-43, the ALS-associated mutation A315T promoted collapsed conformations. In contrast, a canonical passive chaperone, DNAJA2, and a Hero protein, Hero11, both of which prevent TDP-43 aggregation in cells, promoted extended conformations. Our results link single-molecule effects on the TDP-43 conformation to macro effects on bulk aggregation propensity, where a Hero protein, like a canonical chaperone, maintains the conformational integrity of a client protein to prevent its aggregation.

*Keywords*

Heat-resistant obscure (Hero) protein/ Heat shock protein 40 (HSP40)/ prion-like low-complexity domain (LCD)/ total internal reflection fluorescence-based single-molecule fluorescence energy transfer (TIRF-smFRET)/ Transactive response DNA-binding protein 43 (TDP-43)

## Introduction

Every protein has a native state consisting of the set of structural conformations at which it is biologically functional. This can range from one or a few stable structure(s) as classically seen in independently folding domains, to extremely diverse conformational ensembles seen in intrinsically disordered proteins (IDPs). However, there is a vast possibility of structures beyond the native state available for a protein to adopt. For example, proteins regularly undergo some degree of unfolding during normal cellular processes such as protein synthesis, membrane translocation, and other interactions (Knowles *et al*, 2014). Crucially, proteins are also susceptible to misfolding into non-native structures, the rate of which can be increased by aberrant factors such as mutations or errors in protein synthesis, heat or oxidative stress, and cellular aging (Knowles *et al*, 2014; Tyedmers *et al*, 2010). Misfolded proteins typically expose hydrophobic surfaces normally buried in the native state, which are highly prone to bind similar surfaces in other misfolded proteins (Soto, 2003). Left alone, these accumulate into protein aggregates, which are often associated with neurodegenerative diseases such as Alzheimer's disease, Parkinson's disease, and amyotrophic lateral sclerosis (ALS).

Accordingly, cells must suppress protein misfolding and aggregation. Protein chaperones are well-studied machines that actively promote the disassembly and refolding of aggregated proteins to their native state via ATP-dependent mechanisms. Additionally, chaperones are also capable of passive "holdase" mechanisms that prevent misfolding by specifically binding to misfolded proteins. For example, J-domain proteins, also known as DNAJ or HSP40 proteins, can directly and passively chaperone client proteins by themselves, in addition to their better-known co-chaperoning role with active HSP70s that act as ATP-dependent "foldases" (Rosenzweig *et al*, 2019). Holdase binding is thought to stabilize unfolded client proteins, effectively sequestering them away from the aggregation pathway and reducing the burden on ATP-dependent chaperones (Mitra *et al*, 2022). It is thought the ATP-independent nature of passive mechanisms makes them especially advantageous during low growth conditions, suggesting their importance in slow or non-dividing cell types such as neuronal cells (Graff *et al*, 2020).

In addition to chaperones, other passive protein factors also play important roles in stabilizing client proteins. For example, we previously reported that heat-resistant obscure (Hero) proteins, abundant in the boiled supernatant of human and fly cells, also play a role in stabilizing client proteins (Tsuboyama *et al*, 2020). Like chaperones, Hero proteins stabilize activities of client proteins from heat, desiccation, and organic solvent stresses, and even prevent them from aggregation. Yet, unlike chaperones, Hero proteins are highly hydrophilic, electrostatically charged, and intrinsically disordered. Remarkably, Hero protein

activity seems to rely on their biophysical properties as highly charged and sufficiently long polymers, rather than specific sequence-encoded structure. Despite this, we observed that Hero proteins still appear to have different protective effects for different client proteins. Other groups have also independently reported ATP-independent protein chaperoning-like abilities of human-derived IDPs (Huang *et al*, 2021; Ikeda *et al*, 2020). However, it is still unclear how such disordered proteins can suppress aggregation, a role predominately thought to be played by well-structured canonical chaperones.

While IDPs are generally not necessarily prone to aggregate, the aggregation of several IDPs are famously involved in neurodegenerative diseases (Knowles *et al*, 2014; Tompa, 2009). One example is transactive response DNA binding protein 43 kDa (TDP-43), found aggregated in ~97% of amyotrophic lateral sclerosis (ALS) and ~45% of frontotemporal dementia (FTD) cases (Ling *et al*, 2013). At the core of TDP-43 aggregates is its prion-like low complexity domain (LCD), an intrinsically disordered region of 141 amino acids. The LCD is also the site of many ALS-associated point mutations including A315T, R361S, and N390S (Jo *et al*, 2020; Kabashi *et al*, 2008; Prasad *et al*, 2019), which increase TDP-43 aggregation and neurotoxicity in cells (Guo *et al*, 2011; Johnson *et al*, 2009; Nonaka *et al*, 2009). Consistent with the high frequency of disease-causing mutants in LCD, recent structural studies have revealed amyloid fibril structures formed from fragments or the whole LCD *in vitro* and a protease-resistant fragment derived from ALS-FTD patients (Arseni *et al*, 2021; Cao *et al*, 2019; Guenther *et al*, 2018; Li *et al*, 2021). Notably, all these structures are conformationally distinct, suggesting the possibility of different conformational strains in different TDP-43 related diseases, reminiscent of prion strains (Arseni *et al*, 2021; Laferrière *et al*, 2019). In some cases, TDP-43 is known to form amorphous aggregates rather than amyloid fibrils (Jiang *et al*, 2022; Laferrière *et al*, 2019). Altogether these detailed structural studies imply a highly heterogeneous process underlying the aggregation of the TDP-43 LCD.

While protein aggregates give detailed information on the end results of aggregation, there is a lack of information on the highly dynamic and conformationally heterogeneous process preceding the formation of fibrils. These earlier stages of aggregation are important, as neurotoxicity may arise from early oligomeric species of misfolded proteins, including TDP-43 (Wells *et al*, 2021). Crucially, differences in conformational behaviors here are expected to influence how a protein interacts and thus oligomerizes and aggregates. For example, while the TDP-43 LCD is predominantly disordered, the presence of a transient alpha-helical structure is reported to influence self-interactions that modulate the properties of its phase separation (Conicella *et al*, 2020, 2016). However, the early-stage conformational behavior of the overall LCD has remained understudied as these ensemble-averaged studies provide limited insight into

monomeric LCDs before forming phase-separation or aggregation. Additionally, the use of LCD fragments may omit contributions of the domains in full-length TDP-43. Moreover, despite their critical role in suppressing aggregation, it is unclear how chaperones and Hero proteins affect client proteins, and how these compare to the effects of aggregation-promoting mutations.

Here we address this lack of information by studying the effects of a canonical holdase chaperone, DNAJA2, and a Hero protein, Hero11 on the conformation of LCD in full-length TDP-43 using single-molecule fluorescence energy transfer (smFRET) microscopy as well as on bulk aggregation using cell-based assays. While we observed a broad FRET distribution of the LCD indicative of high conformational heterogeneity between molecules, a well-characterized ALS-associated mutation (A315T) in the LCD shifted this towards collapsed conformations. In contrast, despite sequence differences between Hero11 and DNAJA2, both mechanisms resulted in similarly extended LCD conformations. Importantly, the effects of Hero11 and DNAJA2 on the conformational distribution of the LCD correspond to their effects on preventing bulk aggregation. Overall, our study unveils the molecular mechanism of how Hero proteins suppress client protein aggregation despite the lack of structure.

## Results & Discussion

*DNAJA2 and Hero11 suppress TDP-43 aggregation in HEK293T cells*

In order to compare the protective effects of canonical chaperones and Hero proteins at the bulk level, we first performed cell-based aggregation assays (Tsuboyama *et al*, 2020). Since cytoplasmic aggregation of TDP-43 is associated with its pathology (Arai *et al*, 2006; Neumann *et al*, 2006), we used GFP-tagged TDP-43 lacking its nuclear localization signal (GFP-TDP43ΔNLS) to increase cytoplasmic mislocalization and aggregation. GFP-TDP43ΔNLS was co-transfected with Hero proteins, canonical chaperone proteins, or the GST (Glutathione S-transferase) control into HEK293T cells, and aggregation was assessed by the filter trap method (Fig 1A). It was previously reported that, while overexpression of HSP90 increases TDP-43 levels, aggregation, and toxicity in yeast cells (Lin *et al*, 2021), the overexpression of HSP70 suppresses aggregation in HeLa cell nucleus and aggregation of a TDP-43 fragment in mouse cells (Kitamura *et al*, 2018; Udan-Johns *et al*, 2014). Meanwhile, another report has shown that high overexpression of Sti1 in yeast (HOP in humans) increases TDP-43 toxicity, while moderate expression slightly rescues toxicity (Lin *et al*, 2021). In our hands, co-transfection of HSP70 (HSPA8), HSP90 (HSP90AB1), or HOP all failed to suppress TDP-43 aggregation compared to the GST control, possibly because HEK293T cells already express high levels of these chaperones. In contrast, the J-domain protein, DNAJA2, significantly ($p < 0.01$) suppressed aggregation of co-transfected GFP-TDP43ΔNLS compared to the GST control (Fig 1B−D), in line with previous studies that identified different DNAJB subfamily proteins as suppressors of TDP-43 aggregation (Chen *et al*, 2016; Park *et al*, 2017; Udan-Johns *et al*, 2014). We have previously shown that an 11 kDa highly positively charged Hero protein, Hero11 (also known as L10K protein or C19orf53) can suppress TDP-43 aggregation, while its KR→G charge mutant, in which all 21 lysine and 6 arginine residues have been mutated to neutral glycine, fails to suppress aggregation, suggesting the importance of net charge for this effect (Tsuboyama *et al*, 2020). In agreement with these previous results, we could confirm that Hero11 but not Hero11KR→G significantly ($p < 0.01$ and $p > 0.05$, respectively) suppresses aggregation of co-transfected GFP-TDP43ΔNLS compared to GST (Fig 1B−D). Overall, our current data highlight DNAJA2 and Hero11 as efficient suppressors of TDP-43 aggregation.

*Single-molecule observation of TDP-43 LCD conformation*

Given the importance of the LCD for TDP-43 aggregation (Arseni *et al*, 2021; Cao *et al*, 2019; Li *et al*, 2021), we next sought to observe the conformational behavior of this region at the single-molecule level. Total internal reflection fluorescence (TIRF)-based smFRET is particularly useful for isolating and

collecting long-range conformational data of individual IDPs that are difficult to obtain by other methods (Borgia *et al*, 2018; Meng *et al*, 2018; Metskas & Rhoades, 2020), resolving heterogeneity between molecules. Using genetic code expansion in HEK293T cells, we produced full-length TDP-43 with the unnatural amino acid, endo-BCN-L-lysine (endoBCN-K), incorporated at the beginning and the end of the LCD. We then performed site-specific dye-labelling at these two positions with tetrazine-coupled fluorescent dyes, Cy3 (donor) and ATTO647N (acceptor) (Nikić *et al*, 2016, 2015; Tsuboyama *et al*, 2018) (Fig S1). This dual-labeled TDP-43 was immobilized onto PEG-biotinylated glass using an N-terminally encoded HaloTag and illuminated via TIRF to observe the conformational behavior of the TDP-43 LCD (Fig 2A, B). An alternating laser excitation (ALEX) scheme, where two lasers were used to alternately excite the donor and acceptor dyes, was used to select molecules labeled with one Cy3 and one ATTO647 dye, as assessed by dye stoichiometry and one-step photobleaching (Fig 2C, D) (Kapanidis *et al*, 2004; Tsuboyama *et al*, 2018).

In our experimental scheme, higher FRET efficiency occurs when fluorophores are in close proximity, corresponding to relative collapse of the LCD, whereas lower FRET efficiency indicates relative extension. Under incubation with the BSA control, we observed a broad range of FRET signals, with a slight peak at ~0.8, suggesting a very heterogenous conformational distribution of the LCD (Fig 2E). Incubation with DNAJA2 resulted in a very low FRET peak at ~0.0 (Fig 2G), which we confirmed was not due to donor-only signals via ALEX. Strikingly, the addition of Hero11 also caused a similar very low FRET peak (Fig 2H). In contrast, Hero11KR→G mutant did not cause apparent changes in the FRET distribution compared with the BSA control (Fig 2F), consistent with its inability to suppress TDP-43 aggregation in cells (Fig 1B–D). Together, these results demonstrate that, while the TDP-43 LCD is highly heterogenous in conformation, Hero11 and DNAJA2 shift the conformational distribution of TDP-43 LCD towards relatively extended forms.

*DNAJA2 and Hero11 also suppress aggregation of an ALS-associated mutation in the LCD*

While structural studies of ALS-associated TDP-43 mutations A315T and A315E at the fibril level suggest they stabilize amyloid fibril structure and promote irreversibility of low-complexity aromatic-rich kinked segments (Cao *et al*, 2019; Guenther *et al*, 2018), it remains unclear how these affect the molecule prior to fibrilization. Thus, we focused on the effect of the A315T mutation on the LCD conformational distribution. We carried out HEK293T cell-based aggregation assays comparing GFP-TDP43 without LCD mutations (WT) or with the A315T mutation (A315T). Each variant GFP-TDP43 was co-transfected

with Hero11, DNAJA2, GST, or Hero11KR→G (Fig 3A). In control conditions (GST or Hero11KR→G), we observed only a slight or no apparent change in aggregation caused by the A315T mutation (Fig 3B, C). This suggests that the expected increase in aggregation by A315T mutation was masked by saturation in our cell-based co-transfection assay. Nonetheless, co-transfection with Hero11 or DNAJA2 still efficiently suppressed aggregation of the A315T mutant comparable to WT (Fig 3B, C). Thus, Hero11 and DNAJA2 efficiently suppress TDP-43 aggregation regardless of the A315T mutation.

*The ALS-associated mutation in the LCD promotes collapse but remains susceptible to the effects of Hero11 and DNAJA2*

Using genetic code expansion in HEK293T cells, we next produced dye-labelled TDP-43 containing the A315T mutation for smFRET studies. Compared to the WT, LCDs with the A315T mutation displayed a prominent high FRET peak (0.8~0.9) in the BSA control incubation, suggesting that this mutation promotes conformational collapse of the LCD (Fig 4A). This also demonstrates the greater sensitivity of smFRET for detecting differences in behaviors caused by this mutation compared to the bulk cell-based aggregation assay. Similar to WT, addition of Hero11 and DNAJA2 resulted in very low FRET peak signals (~0.0) for the A315T LCD (Fig 4C, D). Unlike the WT LCD, incubation with Hero11KR→G resulted in a very broad FRET signal for A315T LCD, suggesting some interaction, but did not promote the low FRET peak (Fig 4B). Thus, both DNAJA2 and Hero11 cause a specific shift to low FRET signals, suggesting similar conformational extension of the mutant LCD. Together, these results suggest the A315T disease-associated point mutation promotes collapsed conformations but is still susceptible to conformational modulation by Hero11 and DNAJA2.

*Effects at the single-molecule level influence the bulk aggregation of the LCD*

Here we show that Hero11 and DNAJA2, both of which prevent aggregation of TDP-43 in cells (Fig 1B–D, 3A–C), promote relatively extended conformations of the TDP-43 LCD (Fig 2G, H, and Fig 4C, D), while the disease-promoting A315T mutation promotes an opposite collapse (Fig 4A). Accordingly, we propose that Hero11 and DNAJA2 suppress aggregation of TDP-43 by exerting conformational effects on the LCD. Through sequestration to this "stabilized" conformational extended state, Hero11 and DNAJA2 prevent the LCD from assuming aggregation-prone collapsed conformations (Fig 4E), leading to suppressed aggregation at the bulk level (Fig 4F). Our results highlight a mechanism occurring at the single-molecule level that may explain how Hero proteins suppress aggregation.

Our single-molecule observations are consistent with observations at the bulk level. Bulk studies of fibrillar TDP-43 aggregation indicate compaction of the LCD around different hydrophobic core structures (Arseni *et al*, 2021; Cao *et al*, 2019; Li *et al*, 2021). Interestingly, the ALS-associated mutations A315E and A315T promote aggregation by stabilizing these amyloid fibril structures through intra- and inter-strand interactions (Cao *et al*, 2019; Guenther *et al*, 2018). In apparent consistency, we observed that the A315T mutation promotes conformational collapse of the full-length LCD at the single-molecule level, compared to WT LCD. This suggests that, in addition to its effects at the fibril level, A315T mutation also contributes to pathogenicity by causing aberrant conformational behavior of individual LCDs at the single-molecule level. Regardless, Hero11 and DNAJA2 promote extended conformations of the A315T mutant LCD (Fig 4), in line with their ability to suppress aggregation of A315T mutant TDP-43 in cells (Fig 3). Overall, the correlation between smFRET and bulk aggregation suggests that conformational integrity at the single-molecule level is linked to the macroscopic behaviors like bulk aggregation.

*Hero proteins may play a complementary role to canonical chaperones*

Our observation that DNAJA2 stabilizes a conformational state of the TDP-43 LCD is in line with its "holdase" activity as a canonical passive chaperone. Remarkably, despite our inability to detect specific binding between Hero11 and TDP-43 (K.T. and Y.T., unpublished observation), Hero11 maintains a low FRET population of the LCD similar to DNAJA2. The lack of folded structure and poor conservation in Hero protein sequences suggest Hero11 acts without any specific interaction with the LCD. However, this ability to impart conformational effects is dependent on the high positive charge of Hero11, as the

Hero11KR→G mutant failed to elicit effects at both the single-molecule (Figs 2 and 4) and bulk levels (Figs 1 and 3). The importance of net charge for Hero protein function is supported by our observation that net positively charged Hero proteins (Hero11, Hero7, and Hero45), but not net negatively charged Hero proteins (Hero9, Hero13, Hero20), suppress TDP-43 aggregation (Tsuboyama *et al*, 2020). Altogether this suggests that Hero proteins may use a distinct mode of action, dependent on its biophysical property as a charged polymer instead of folded structure, to modulate client protein conformation and aggregation.

Despite their different properties, Hero proteins appear to have similar biological effects as conventional chaperones. For example, we previously showed that overexpression of Hero protein extends the lifespan of flies, and protects client protein activity in cells, similar to the effects of conventional chaperones (Tsuboyama *et al*, 2020). Here, we demonstrate that Hero proteins display similar effects as a canonical HSP40 chaperone on the aggregation pathway of TDP-43. This suggests that like canonical chaperones, Hero proteins can maintain the conformational integrity of client proteins, which may result in the overall fitness of the cell. This mechanism may also explain how other highly charged, intrinsically disordered proteins show apparent chaperone-like effects (Huang *et al*, 2021; Ikeda *et al*, 2020). Overall, we envision that the protective abilities of Hero proteins complement those of the conventional chaperones, reinforcing the conformational health of the proteome.

**Figure legends**

*Figure 1 - DNAJA2 and Hero11 suppress aggregation of TDP-43 in HEK293T cells*

A Schematic of the HEK293T cell-based filter trap assay for TDP-43 aggregation. Plasmids for GFP-TDP43ΔNLS and the indicated protein were co-transfected into HEK293T cells and incubated for 48 h. Cells were lysed, and aggregates captured on 0.2 μm filter membrane for detection via immunoblotting for GFP.

B Representative microscope images of GFP signals in HEK293T cells. Images from a single independent repeat are shown.

C Immunoblots for aggregated GFP-TDP43ΔNLS in HEK293T cells detected with α-GFP antibody. For each filter trap membrane (n = 3 independent experiments), each sample is loaded three times at two-fold serial dilution.

D Quantification of TDP-43 aggregation in (C) via densitometry of the highest concentration samples. Bar plots represent the mean and 95% confidence intervals as the bar heights and error bars, respectively. Dots represent the values of individual experiments. **, $p < 0.01$; ***, $p < 0.001$; otherwise, $p \geq 0.05$ (Dunnett's test, GST control).

*Figure 2 - Single-molecule FRET observation of the TDP-43 LCD*

A Schematic of TIRF-based single-molecule FRET observation of the LCD (orange) on full-length TDP-43. Note that while the donor (green) and acceptor dyes (red) are randomly incorporated at the two sites, only donor/acceptor-labelled molecules were selected for analysis (see methods).

B Representative smFRET microscope images (from DNAJA2 incubation). Donor (left) and acceptor (middle) emissions under donor excitation are displayed in pseudo-color, as indicated by the colormap. Both donor (colored green) and acceptor (colored red) images are merged in the Both image (right). The same example molecule is circled in all three images.

C, D Representative FRET traces selected for analysis from Hero11KR→G (C) and Hero11 (D) incubation. The left y-axis in the upper panel corresponds to fluorescence intensity of the Cy3 donor signal (green) and ATTO647N acceptor signal (red) under donor excitation (Intensity D. Ex.). The right y-axis in the upper panel corresponds to FRET efficiency (E, cyan) until first photobleaching event (grey shading). The left y--axis in the lower panel corresponds to fluorescence intensity of the ATTO647N acceptor signal (red) under acceptor excitation (Intensity A. Ex.). The right y--axis in the lower panel corresponds to dye stoichiometry (S, magenta). In (D), a FRET efficiency value below –0.1, derived from donor blinking, is excluded from the trace for clarity.

E – H FRET efficiency distribution of the TDP-43 LCD under incubation in BSA (E), Hero11KR→G (F), DNAJA2 (G), or Hero11 (H). Density plots represent mean ± SEM, as the solid lines and shaded areas, respectively (n = 3 independent experiments). Histograms contain all observations from independent experiments. The total number of molecules in each histogram are: BSA (E), 150; Hero11KR→G (F), 160; DNAJA2 (G), 178; and Hero11 (H), 168.

*Figure 3 - DNAJA2 and Hero11 suppress aggregation of TDP-43 with the A315T mutation*

A Representative microscope images of GFP signals in HEK293T cells co-transfected with plasmids for TDP43ΔNLS with or without a mutation in the LCD (WT or A315T, respectively) and the indicated protein.

B Immunoblots for aggregated GFP-TDP43ΔNLS variants in HEK293T cells detected with α-GFP antibody. For each filter trap membrane (n = 3 independent experiments), each sample is loaded three times at two-fold serial dilution.

C Quantification of TDP-43 aggregation in (B) via densitometry of the highest concentration samples. Bar plots represent the mean and 95% confidence intervals as the bar heights and error bars, respectively. Bar color indicates the co-transfected protein, according to the legend on the bottom. Dots represent the values of individual experiments. Within each variant **, $p < 0.01$; ***, $p < 0.001$; otherwise, $p \geq 0.05$ (Dunnett's test, GST control).

*Figure 4 - Single-molecule FRET observation of the TDP-43 LCD with the A315T mutation*

A – D FRET efficiency distribution of the TDP-43 LCD bearing the A315T mutation under incubation in BSA (A, lower panel), Hero11KR→G (B), DNAJA2 (C), or Hero11 (D). Density plots represent mean ± SEM, as the solid lines and shaded areas, respectively (n = 3 independent experiments). Histograms contain all observations from independent experiments. The number of molecules in the lower four histograms are as follows: BSA (A, lower panel), 101; Hero11KR→G (B), 255; DNAJA2 (C), 357; and Hero11 (D), 216. Fig 2E is replotted (A, upper panel) as a reference for the behavior of TDP-43 with WT LCD under BSA incubation.

E, F Model for how conformational effects on the TDP-43 LCD at the single-molecule level (E) relate to effects on aggregation at the bulk level (F). At the level of individual molecules (E), the TDP-43 LCD populates a broad conformational ensemble (orange). Hero proteins (blue, Hero11) and JDPs (green, DNAJA2) promote extended conformations, whereas disease-associated mutations (brown arrow) promote collapsed conformations. At the bulk level of many molecules (F), extended conformations lead to non-aggregated TDP-43 (teal downwards arrow). Meanwhile, collapsed conformations lead to TDP-43 aggregation (brown downwards arrow).

*Supplementary Figure 1 - Genetic code expansion in HEK293T cells for dye-labelling of TDP-43*

A Schematic of HALO-TDP43 with unnatural amino acids incorporated around the LCD after elution via TEV protease cleavage. Boxes indicate TDP-43 regions and tags: N-terminal domain (NTD), two RNA recognition motifs (RRM1 and RRM2), low-complexity domain (LCD), HaloTag, and 2xHA tag. Numbers indicate the amino acids of TDP-43 based on the numbering used in a previous study (Cao *et al*, 2019). The last amino acid of the HaloTag is the 23$^{rd}$ amino acid from the start of the TDP-43 sequence. Sites of unnatural amino acid (endo BCN-L-Lysine) incorporation are indicated by the violet boxes. Arginine 268 was replaced with endo BCN-L-Lysine, while the other site was incorporated into a linker at the 6$^{th}$ amino acid after the LCD sequence, before a 2×HA-tag. The yellow triangle marks A315.

B Amino acid sequence of (A). Highlight color corresponds to the regions in (A). The N-terminal glycine is left over from the TEV protease cleavage, the asterisk marks the end of the sequence. A315 is indicated in yellow.

C Dye-labeling of HALO-TDP43. HEK293T cells expressing FLAG-tev-HALO-TDP43 incorporated with unnatural amino acids were lysed and incubated on anti-FLAG Dynabeads. Proteins were dye-labeled on bead and eluted via cleavage with TEV protease in naïve HEK293T cell lysate (note the multiple bands in the elution fraction of the CBB stain). Copper-free click chemistry-based, dye-labeling of endo BCN-L-Lysine with tetrazine-Cy3 (Donor) and tetrazine-ATTO-647N (Acceptor) was confirmed by fluorescence imaging in gel with excitation at 520 nm and 620 nm, respectively, before staining with Coomassie Brilliant Blue (CBBS). The two bands in Elution fraction correspond to HALO-TDP43 with only one or two dyes incorporated (lower and upper bands, respectively). The Beads fraction indicates proteins that did not elute from the Dynabeads, and the higher molecular weights likely correspond to dye-labelled but uncleaved FLAG-tev-HALO-TDP43.

## Materials and Methods

*HEK293T Cell culture and lysate preparation*

HEK293T cells were maintained in Dulbecco's Modified Eagle Medium (DMEM, Sigma, QJ-D6429) supplemented with 10% FBS in a 5% $CO_2$ atmosphere at 37°C. Naïve HEK293T cell lysates were produced as previously described (Tsuboyama *et al*, 2020).

*Plasmid preparation*

*Plasmids for recombinant protein production in E. coli*

Plasmids for recombinant expression of Hero proteins and control, pColdI_ Hero11, Hero11KR→G, and GST -FLAG-6×His were previously described (Tsuboyama *et al*, 2020). Recombinant plasmids for chaperones pColdI_6×His- DNAJA2, HOP, and HSPA8 were previously described (Naruse *et al*, 2018).

*Plasmids for HEK293T cell-based assays and protein production*

For transfection into HEK293T cells, pCAGEN_6×His- DNAJA2-HA and HOP-HA were created by PCR of ORFs from pColdI_6×His- DNAJA2 and HOP, respectively, and insertion into EcoRI-digested pCAGEN plasmids using NEBuilder HiFi DNA Assembly Master Mix (NEB). Plasmids for Hero protein and controls, pCAGEN_FLAG- Hero11, Hero11KR→G, and GST were previously described (Tsuboyama *et al*, 2020). Plasmids for canonical chaperones, pCAGEN_SBP-HSPA8, HSP90AB1, DNAJB8 and DNAJC8 were created as previously described (Iwasaki *et al*, 2015). Plasmids for genetic code expansion, pCAGEN_U6tRNAUCmut×4_NESPylRS-Afmut and pCAGEN_U6tRNAUCmut×4_eRF1EDmut were previously described (Tsuboyama *et al*, 2018). Plasmids for expression of GFP-tagged TDP-43 in HEK293T cells, pCAGEN_eGFP-TDP43 and TDP43ΔNLS were previously described (Tsuboyama *et al*, 2020). The plasmid for incorporating unnatural amino acids in TDP-43, pCAGEN_FLAG-TEV-HALO-TDP43_R268Amb-F420Amb-2×HA-Och was created first by PCR of the ORF from pCAGEN_eGFP- TDP43 and insertion into NotI-digested pCAGEN_FLAG-tev-HALO-Ago2. Then an ocher mutation of the final stop codon after 2×HA, and amber mutations around the TDP-43 LCD at R268 and F420 were introduced by PCR-based site-directed mutagenesis, as previously described (Tsuboyama *et al*, 2018). For testing the A315T mutation, pCAGEN_eGFP-TDP43_A315T, pCAGEN_eGFP-TDP43_A315TΔNLS, and pCAGEN_FLAG-TEV-HALO-TDP43_R268Amb-A315T-F420Amb-2×HA-Och were created from A315T mutation of pCAGEN_eGFP-TDP43, pCAGEN_eGFP-TDP43_ΔNLS, and pCAGEN_FLAG-TEV-HALO-TDP43_R268Amb-F420Amb-2×HA-Och, respectively, via PCR-based site-directed mutagenesis.

*Protein Preparation*

*Protein Purification of His-tagged proteins from pColdI plasmids.*

Recombinant Hero proteins and charge mutants and DNAJA2 were purified as previously described (Naruse *et al*, 2018; Tsuboyama *et al*, 2020). Briefly, pColdI plasmids for FLAG-6×His-tagged proteins were transfected in Rosetta2 (DE3) and grown at 37°C to O.D. 0.4−0.6. Proteins were induced with 1 mM isopropyl-β-D-thiogalactoside (IPTG) overnight at 15°C and snap-frozen with liquid nitrogen. Cells were lysed by probe sonication in His A buffer (30 mM HEPES-KOH pH 7.4, 200 mM KOAc, 2 mM $Mg(OAc)_2$, 5% glycerol) supplemented with cOmplete™, EDTA-free Protease Inhibitor Cocktail (Roche), cleared by centrifugation, and purified over Ni-NTA resin (Roche) and eluted with His B buffer (HisA with 400mM imidazole). Proteins were buffer exchanged into 1×PBS using PD-10 columns (Cytiva), concentration determined by BCA assay (Pierce) before supplementation with 1 mM DTT, snap frozen in aliquots and stored at −80°C.

*Protein purification via genetic code expansion*

Genetic code expansion was performed as described previously (Tsuboyama *et al*, 2018). HEK293T cells were seeded and transfected after 24 h with pCAGEN plasmids in medium, EndoBCN-K (SiChem, SC-8014) supplemented, and harvested 48 h after transfection. Cells were lysed via BIORUPTOR II (BM Bio), snap-frozen with liquid nitrogen and stored at −80°C. Proteins were purified with FLAG-functionalized Dynabeads Protein G (Invitrogen), dye-labelled on beads with tetrazine functionalized-Cy3 and ATTO647N (Jena Bioscience, CLK-014-05 and CLK-012-02), functionalized with HaloTag Biotin ligand (Promega, G8281), eluted in naïve HEK293T cell lysate with TurboTEV Protease (Accelagen, T0102S), and aliquots snap-frozen in liquid nitrogen and stored at −80°C. Fluorescent dye-labelling was verified on SDS-PAGE via detection of fluorescence at indicated wavelengths with an Imager 600 (Amersham).

*Cell-based aggregation assays*

Cell-based aggregation assays were performed as previously described (Tsuboyama *et al*, 2020). HEK293T cells were co-transfected with 200 ng pCAGEN plasmid for TDP-43 and 1000 ng pCAGEN plasmid for the other protein using Lipofectamine™ 3000 Transfection Reagent (Invitrogen, L3000001) in 12-well plates. After 48 h, cells were imaged using FLUOVIEW FV3000 confocal laser scanning microscope (Olympus) and then lysed with BIORUPTOR II (BM Bio) in 1xPBS supplemented 1x

cOmplete™ Protease Inhibitor Cocktail (Roche) in Protein LoBind® Tubes (Eppendorf). Protein levels were normalized via Bradford assay (Bio-Rad) and aggregates were captured on a 0.2 μm Whatman OE66 cellulose acetate membrane filter (GE Healthcare, 10404180) using 1× PBS with 1% SDS to solubilize. TDP-43 aggregation levels were detected by GFP fluorescence signal and immunoblotting for GFP using α-GFP (B-2) primary antibody (Santa Cruz Biotechnology, sc-9996) with α-mouse IgG secondary antibody (MBL).

*Single-molecule FRET assay*

Single-molecule assays were conducted as previously described (Sasaki *et al*, 2018; Tsuboyama *et al*, 2018), with modifications to minimize aggregation. Aliquots of dye-labelled HALO-TDP43 were pre-diluted in 1×Lysis buffer (30 mM HEPES-KOH pH 7.4, 100 mM KOAc, 2 mM $Mg(OAc)_2$), and then diluted in naïve HEK293T cell lysate with 1×ATP regeneration system (1 mM ATP, 25 mM creatine monophosphate (Sigma), 0.03 U/μL creatine kinase (Calbiochem), 0.1 U/μL RNasin Plus RNase Inhibitor (Promega), in Lysis buffer) and incubated at 37°C for 30 min, to enable aggregation-clearing chaperone activities. Note the use of high-quality HEK293T cell lysate via hypotonic lysis method was crucial, as lysate prepared via sonication failed to sufficiently remove aggregates. This disaggregation reaction was then centrifuged at 18,000 × G for 15 min at 25°C and supernatant collected to remove aggregated proteins in the pellet. Observation chambers were prepared as previously described (Sasaki *et al*, 2018; Tsuboyama *et al*, 2018) infused with neutravidin for 2 min, and washed with Lysis buffer. Supernatant was flowed into chamber and incubated for 2 min, and then washed twice with Wash buffer (1×Lysis buffer containing 1% Triton X-100 and 800 mM NaCl), four times with Wash buffer supplemented with 10 mM ATP, and then four times with Lysis buffer. These stringent washes are necessary to remove nonspecific interactions and oligomerization of TDP-43 with the tethered TDP-43 molecules. The final Observation buffer containing 0.3 g/L of BSA or recombinant protein in 1× PBS with 1 mM DTT, $O_2$ scavenger system (7.1 mM PCA (3,4-Dihydroxybenzoic acid, 37580, Sigma) with 29 nM PCD (Protocatechuate 3,4-dioxygenase, P8279, Sigma) (Aitken *et al*, 2008)), and 2 mM Trolox (6-hydroxy-2,5,7,8-tetramethylchroman-2-carboxylic acid, 238813, Sigma) was flowed into chamber and then mounted onto microscope stage for smFRET observations. Three five-minute videos were taken of each slide, using alternating laser illumination of 1s each. We emphasize that these changes are uniquely practical for TIRF-smFRET experiments, which by tethering dye-labelled molecules, allows for buffer exchange of an extremely small sample.

*Image processing and quantification*

*Microscope Imaging*

The live HEK293T cell images from FLUOVIEW FV3000 confocal laser scanning microscope (Olympus) in Figs 1 and 3 were produced using the QuickFigs plugin (Mazo, 2021) in Fiji (Schindelin *et al*, 2012).

*Analysis of aggregation assays*

Images from bulk aggregation filter trap assays in Figs 1 and 3 were taken using Amersham ImageQuant 800 Imager (Amersham), in TIFF image format. For quantification, images were analyzed using ImageJ in a manner similar to dot blots, first with background subtraction via the "Subtract Background" tool, with a rolling ball radius of 40 pixels. Circular areas of 146-pixels diameter were selected around the highest concentration wells to obtain integrated densities for each sample. This was repeated for three independent experiments ($n = 3$) and saved to CSV file format. Statistics were conducted with R 4.2.1, using RStudio Desktop 2022.07.1+554 IDE. For Fig 1, a one-way ANOVA was performed to compare the effect of the different co-transfections on the aggregation of co-transfected TDP-43, indicating a statistically significant difference between at least two groups ($p < 0.001$). Significant differences in mean aggregation compared to the GST control were assessed for each condition via Dunnett's test for comparing several treatments with a control. For Fig 3, one-way ANOVA tests were performed on each TDP-43 variant, to compare the effect of different co-transfections on the aggregation of the TDP-43 variant ($p < 0.001$ for all variants). For each TDP-43 variant, significant differences in mean aggregation compared to the GST control were assessed for each condition via Dunnett's test. Visualization was conducted with Python 3.7, using Spyder 5 IDE. The pandas library was used to load CSV files as DataFrame objects and plotted as barplots showing the mean and 95% confidence intervals using seaborn.

*Analysis of smFRET assays*

For smFRET-related data in Figs 2 and 3, five-minute videos were taken of each slide and saved in FITS file format. Videos were imported to iSMS implemented in MATLAB for image channel alignment, peak localization, FRET-pair identification, photobleaching and blinking identification, drift correction, and correction factor determination and application as previously described (Preus *et al*, 2015; Tsuboyama *et al*, 2018). FRET efficiency traces were selected based on single-step photobleaching, stoichiometry ~0.4 via ALEX and anticorrelation. FRET distribution analysis data were exported as TXT files from iSMS.

This process was repeated in three independent experiments for each condition (n = 3). Visualization was conducted through Python 3.7, using Spyder 5 IDE. The pandas library was used to load TXT files as DataFrame objects and density histograms were plotted using the combined data for each condition via seaborn, with 25 bins. Average density plots were created by estimating the probability density functions for each independent experiment via gaussian kernel density estimation with 0.05 bandwidth using SciPy, and values of each curve evaluated for determination of means and standard errors along the entire range. Mean density and standard error of the mean for each condition were plotted using matplotlib over the histograms.

**Data Availability**

Data are available from the authors upon reasonable request.

**Acknowledgments**

We thank all members of the Tomari laboratory for critical comments on the manuscript. This work was supported in part by JSPS KAKENHI Grant-in-Aid for Transformative Research Areas (A) 21H05278 (to Y. T.), Grant-in-Aid for Scientific Research (S) 18H05271 (to Y. T.) and Grant-in-Aid for JSPS Fellows 22J11678 (to A. Y. W. L.).

**Conflict of interest**

Y. T. and K. T. have patent applications related to this work. H. T. and A. Y. W. L. declare no competing interests.

**References**

Aitken CE, Marshall RA & Puglisi JD (2008) An Oxygen Scavenging System for Improvement of Dye Stability in Single-Molecule Fluorescence Experiments. *Biophysical Journal* 94: 1826–1835

Arai T, Hasegawa M, Akiyama H, Ikeda K, Nonaka T, Mori H, Mann D, Tsuchiya K, Yoshida M, Hashizume Y, *et al* (2006) TDP-43 is a component of ubiquitin-positive tau-negative inclusions in frontotemporal lobar degeneration and amyotrophic lateral sclerosis. *Biochemical and Biophysical Research Communications* 351: 602–611

Arseni D, Hasegawa M, Murzin AG, Kametani F, Arai M, Yoshida M, Ryskeldi-Falcon B, Hasegawa M, Murzin AG, Kametani F, *et al* (2021) Structure of pathological TDP-43 filaments from ALS with FTLD. *Nature*: 1–5

Borgia A, Borgia MB, Bugge K, Kissling VM, Heidarsson PO, Fernandes CB, Sottini A, Soranno A, Buholzer KJ, Nettels D, *et al* (2018) Extreme disorder in an ultrahigh-affinity protein complex. *Nature* 555: 61–66

Cao Q, Boyer DR, Sawaya MR, Ge P & Eisenberg DS (2019) Cryo-EM structures of four polymorphic TDP-43 amyloid cores. *Nat Struct Mol Biol* 26: 619–627

Chen H-J, Mitchell JC, Novoselov S, Miller J, Nishimura AL, Scotter EL, Vance CA, Cheetham ME & Shaw CE (2016) The heat shock response plays an important role in TDP-43 clearance: evidence for dysfunction in amyotrophic lateral sclerosis. *Brain* 139: 1417–1432

Conicella AE, Dignon GL, Zerze GH, Schmidt HB, D'Ordine AM, Kim YC, Rohatgi R, Ayala YM, Mittal J & Fawzi NL (2020) TDP-43 α-helical structure tunes liquid–liquid phase separation and function. *PNAS* 117: 5883–5894

Conicella AE, Zerze GH, Mittal J & Fawzi NL (2016) ALS Mutations Disrupt Phase Separation Mediated by α-Helical Structure in the TDP-43 Low-Complexity C-Terminal Domain. *Structure* 24: 1537–1549

Graff AM de, Mosedale DE, Sharp T, Dill KA & Grainger DJ (2020) Proteostasis is adaptive: Balancing chaperone holdases against foldases. *PLOS Computational Biology* 16: e1008460

Guenther EL, Cao Q, Trinh H, Lu J, Sawaya MR, Cascio D, Boyer DR, Rodriguez JA, Hughes MP & Eisenberg DS (2018) Atomic structures of TDP-43 LCD segments and insights into reversible or pathogenic aggregation. *Nat Struct Mol Biol* 25: 463–471

Guo W, Chen Y, Zhou X, Kar A, Ray P, Chen X, Rao EJ, Yang M, Ye H, Zhu L, *et al* (2011) An ALS-associated mutation affecting TDP-43 enhances protein aggregation, fibril formation and neurotoxicity. *Nature Structural & Molecular Biology* 18: 822–830

Huang L, Agrawal T, Zhu G, Yu S, Tao L, Lin J, Marmorstein R, Shorter J, Yang X, Agrawal T, *et al* (2021) DAXX represents a new type of protein-folding enabler. *Nature*: 1–6

Ikeda K, Suzuki S, Shigemitsu Y, Tenno T, Goda N, Oshima A & Hiroaki H (2020) Presence of intrinsically disordered proteins can inhibit the nucleation phase of amyloid fibril formation of Aβ(1–42) in amino acid sequence independent manner. *Scientific Reports* 10: 12334

Iwasaki S, Sasaki HM, Sakaguchi Y, Suzuki T, Tadakuma H & Tomari Y (2015) Defining fundamental steps in the assembly of the Drosophila RNAi enzyme complex. *Nature* 521: 533–536

Jiang YX, Cao Q, Sawaya MR, Abskharon R, Ge P, DeTure M, Dickson DW, Fu JY, Ogorzalek Loo RR, Loo JA, *et al* (2022) Amyloid fibrils in disease FTLD-TDP are composed of TMEM106B not TDP-43. *Nature*: 1–10

Jo M, Lee S, Jeon Y-M, Kim S, Kwon Y & Kim H-J (2020) The role of TDP-43 propagation in neurodegenerative diseases: integrating insights from clinical and experimental studies. *Experimental & Molecular Medicine*: 1–11

Johnson BS, Snead D, Lee JJ, McCaffery JM, Shorter J & Gitler AD (2009) TDP-43 Is Intrinsically Aggregation-prone, and Amyotrophic Lateral Sclerosis-linked Mutations Accelerate Aggregation and Increase Toxicity. *J Biol Chem* 284: 20329–20339

Kabashi E, Valdmanis PN, Dion P, Spiegelman D, McConkey BJ, Velde CV, Bouchard J-P, Lacomblez L, Pochigaeva K, Salachas F, *et al* (2008) TARDBP mutations in individuals with sporadic and familial amyotrophic lateral sclerosis. *Nat Genet* 40: 572–574

Kapanidis AN, Lee NK, Laurence TA, Doose S, Margeat E & Weiss S (2004) Fluorescence-aided molecule sorting: Analysis of structure and interactions by alternating-laser excitation of single molecules. *PNAS* 101: 8936–8941

Kitamura A, Iwasaki N & Kinjo M (2018) Molecular chaperone HSP70 prevents formation of inclusion bodies of the 25-kDa C-terminal fragment of TDP-43 by preventing aggregate accumulation. *Cell Stress and Chaperones* 23: 1177–1183

Knowles TPJ, Vendruscolo M & Dobson CM (2014) The amyloid state and its association with protein misfolding diseases. *Nat Rev Mol Cell Biol* 15: 384–396

Laferrière F, Maniecka Z, Pérez-Berlanga M, Hruska-Plochan M, Gilhespy L, Hock E-M, Wagner U, Afroz T, Boersema PJ, Barmettler G, *et al* (2019) TDP-43 extracted from frontotemporal lobar degeneration subject brains displays distinct aggregate assemblies and neurotoxic effects reflecting disease progression rates. *Nat Neurosci* 22: 65–77

Li Q, Babinchak WM & Surewicz WK (2021) Cryo-EM structure of amyloid fibrils formed by the entire low complexity domain of TDP-43. *Nat Commun* 12: 1620

Lin LT-W, Razzaq A, Di Gregorio SE, Hong S, Charles B, Lopes MH, Beraldo F, Prado VF, Prado MAM & Duennwald ML (2021) Hsp90 and its co-chaperone Sti1 control TDP-43 misfolding and toxicity. *The FASEB Journal* 35: e21594

Ling S-C, Polymenidou M & Cleveland DW (2013) Converging Mechanisms in ALS and FTD: Disrupted RNA and Protein Homeostasis. *Neuron* 79: 416–438

Mazo G (2021) QuickFigs: A toolkit and ImageJ PlugIn to quickly transform microscope images into scientific Figs. *PLOS ONE* 16: e0240280

Meng F, Bellaiche MMJ, Kim J-Y, Zerze GH, Best RB & Chung HS (2018) Highly Disordered Amyloid-β Monomer Probed by Single-Molecule FRET and MD Simulation. *Biophysical Journal* 114: 870–884

Metskas LA & Rhoades E (2020) Single-Molecule FRET of Intrinsically Disordered Proteins. *Annual Review of Physical Chemistry* 71: null

Mitra R, Wu K, Lee C & Bardwell JCA (2022) ATP-Independent Chaperones. *Annual Review of Biophysics* 51: 409–429

Naruse K, Matsuura-Suzuki E, Watanabe M, Iwasaki S & Tomari Y (2018) In vitro reconstitution of chaperone-mediated human RISC assembly. *RNA* 24: 6–11

Neumann M, Sampathu DM, Kwong LK, Truax AC, Micsenyi MC, Chou TT, Bruce J, Schuck T, Grossman M, Clark CM, *et al* (2006) Ubiquitinated TDP-43 in Frontotemporal Lobar Degeneration and Amyotrophic Lateral Sclerosis. *Science* 314: 130–133

Nikić I, Estrada Girona G, Kang JH, Paci G, Mikhaleva S, Koehler C, Shymanska NV, Ventura Santos C, Spitz D & Lemke EA (2016) Debugging Eukaryotic Genetic Code Expansion for Site-Specific Click-PAINT Super-Resolution Microscopy. *Angewandte Chemie International Edition* 55: 16172–16176

Nikić I, Kang JH, Girona GE, Aramburu IV & Lemke EA (2015) Labeling proteins on live mammalian cells using click chemistry. *Nature Protocols* 10: 780–791

Nonaka T, Kametani F, Arai T, Akiyama H & Hasegawa M (2009) Truncation and pathogenic mutations facilitate the formation of intracellular aggregates of TDP-43. *Human Molecular Genetics* 18: 3353–3364

Park S-K, Hong JY, Arslan F, Kanneganti V, Patel B, Tietsort A, Tank EMH, Li X, Barmada SJ & Liebman SW (2017) Overexpression of the essential Sis1 chaperone reduces TDP-43 effects on toxicity and proteolysis. *PLOS Genetics* 13: e1006805

Prasad A, Bharathi V, Sivalingam V, Girdhar A & Patel BK (2019) Molecular Mechanisms of TDP-43 Misfolding and Pathology in Amyotrophic Lateral Sclerosis. *Front Mol Neurosci* 12

Preus S, Noer SL, Hildebrandt LL, Gudnason D & Birkedal V (2015) iSMS: single-molecule FRET microscopy software. *Nature Methods* 12: 593–594

Rosenzweig R, Nillegoda NB, Mayer MP, Bukau B, Nillegoda NB, Mayer MP & Bukau B (2019) The Hsp70 chaperone network. *Nature Reviews Molecular Cell Biology* 20: 665–680

Sasaki HM, Tadakuma H & Tomari Y (2018) Single-Molecule Analysis for RISC Assembly and Target Cleavage. In *Argonaute Proteins: Methods and Protocols*, Okamura K & Nakanishi K (eds) pp 145–164. New York, NY: Springer

Schindelin J, Arganda-Carreras I, Frise E, Kaynig V, Longair M, Pietzsch T, Preibisch S, Rueden C, Saalfeld S, Schmid B, *et al* (2012) Fiji: an open-source platform for biological-image analysis. *Nat Methods* 9: 676–682

Soto C (2003) Unfolding the role of protein misfolding in neurodegenerative diseases. *Nat Rev Neurosci* 4: 49–60

Tompa P (2009) Structural disorder in amyloid fibrils: its implication in dynamic interactions of proteins. *The FEBS Journal* 276: 5406–5415

Tsuboyama K, Osaki T, Matsuura-Suzuki E, Kozuka-Hata H, Okada Y, Oyama M, Ikeuchi Y, Iwasaki S & Tomari Y (2020) A widespread family of heat-resistant obscure (Hero) proteins protect against protein instability and aggregation. *PLOS Biology* 18: e3000632

Tsuboyama K, Tadakuma H & Tomari Y (2018) Conformational Activation of Argonaute by Distinct yet Coordinated Actions of the Hsp70 and Hsp90 Chaperone Systems. *Molecular Cell* 70: 722-729.e4

Tyedmers J, Mogk A & Bukau B (2010) Cellular strategies for controlling protein aggregation. *Nat Rev Mol Cell Biol* 11: 777–788

Udan-Johns M, Bengoechea R, Bell S, Shao J, Diamond MI, True HL, Weihl CC & Baloh RH (2014) Prion-like nuclear aggregation of TDP-43 during heat shock is regulated by HSP40/70 chaperones. *Hum Mol Genet* 23: 157–170

Wells C, Brennan S, Keon M & Ooi L (2021) The role of amyloid oligomers in neurodegenerative pathologies. *International Journal of Biological Macromolecules* 181: 582–604

Figure 1

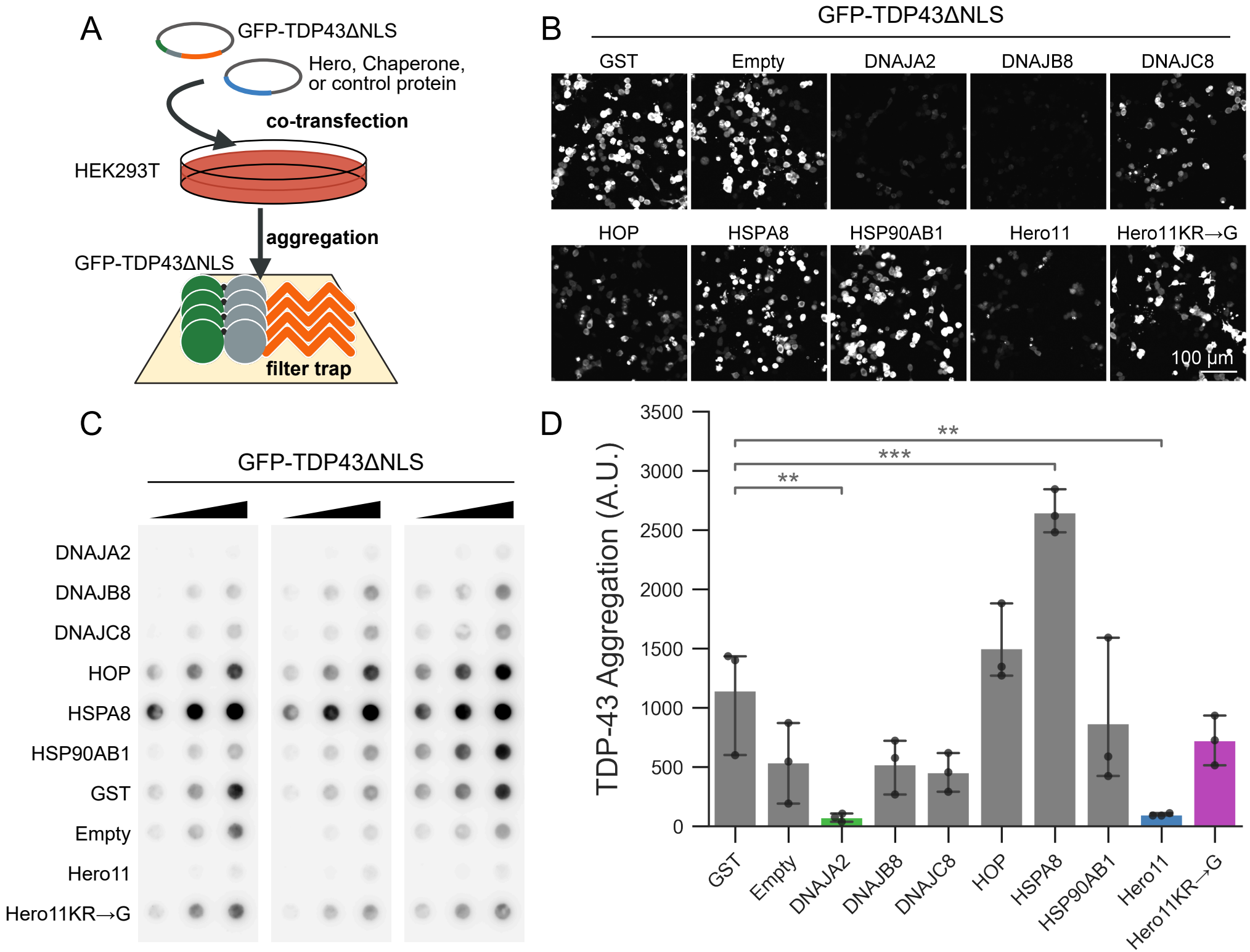
A
GFP-TDP43ΔNLS
Hero, Chaperone, or control protein
co-transfection
HEK293T
aggregation
GFP-TDP43ΔNLS
filter trap
B
GFP-TDP43ΔNLS
GST
Empty
DNAJA2
DNAJB8
DNAJC8
HOP
HSPA8
HSP90AB1
Hero11
Hero11KR→G
100 µm
C
GFP-TDP43ΔNLS
DNAJA2
DNAJB8
DNAJC8
HOP
HSPA8
HSP90AB1
GST
Empty
Hero11
Hero11KR→G
D
TDP-43 Aggregation (A.U.)
3500
3000
2500
2000
1500
1000
500
0
**
***
**
GST
Empty
DNAJA2
DNAJB8
DNAJC8
HOP
HSPA8
HSP90AB1
Hero11
Hero11KR→G

Figure 2

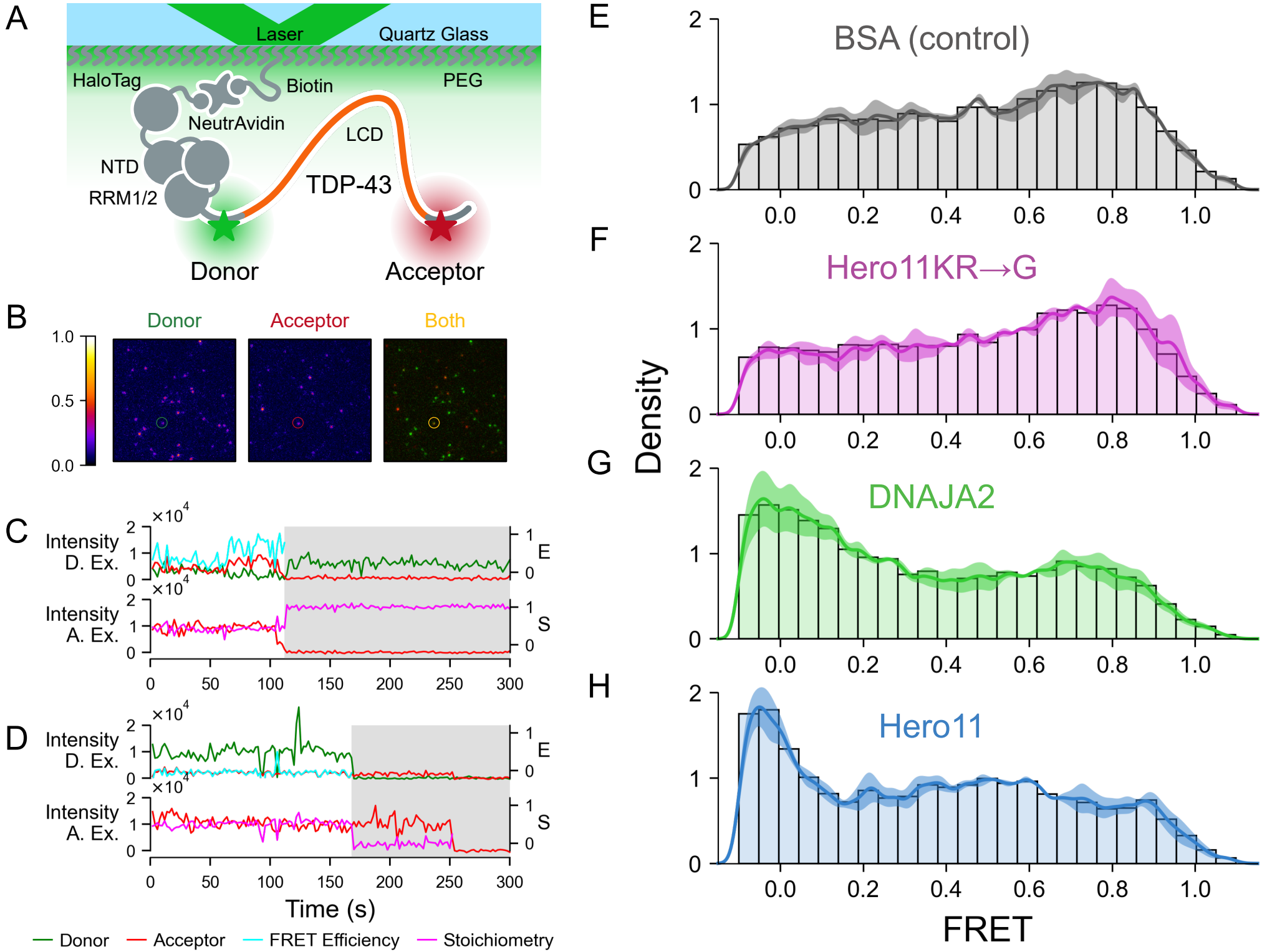
A
Laser
Quartz Glass
HaloTag
Biotin
PEG
NeutrAvidin
LCD
NTD
TDP-43
RRM1/2
Donor
Acceptor
B
Donor
Acceptor
Both
1.0
0.5
0.0
C
Intensity D. Ex.
Intensity A. Ex.
E
S
D
Time (s)
Donor
Acceptor
FRET Efficiency
Stoichiometry
E
BSA (control)
F
Hero11KR→G
G
DNAJA2
H
Hero11
Density
FRET

Figure 3

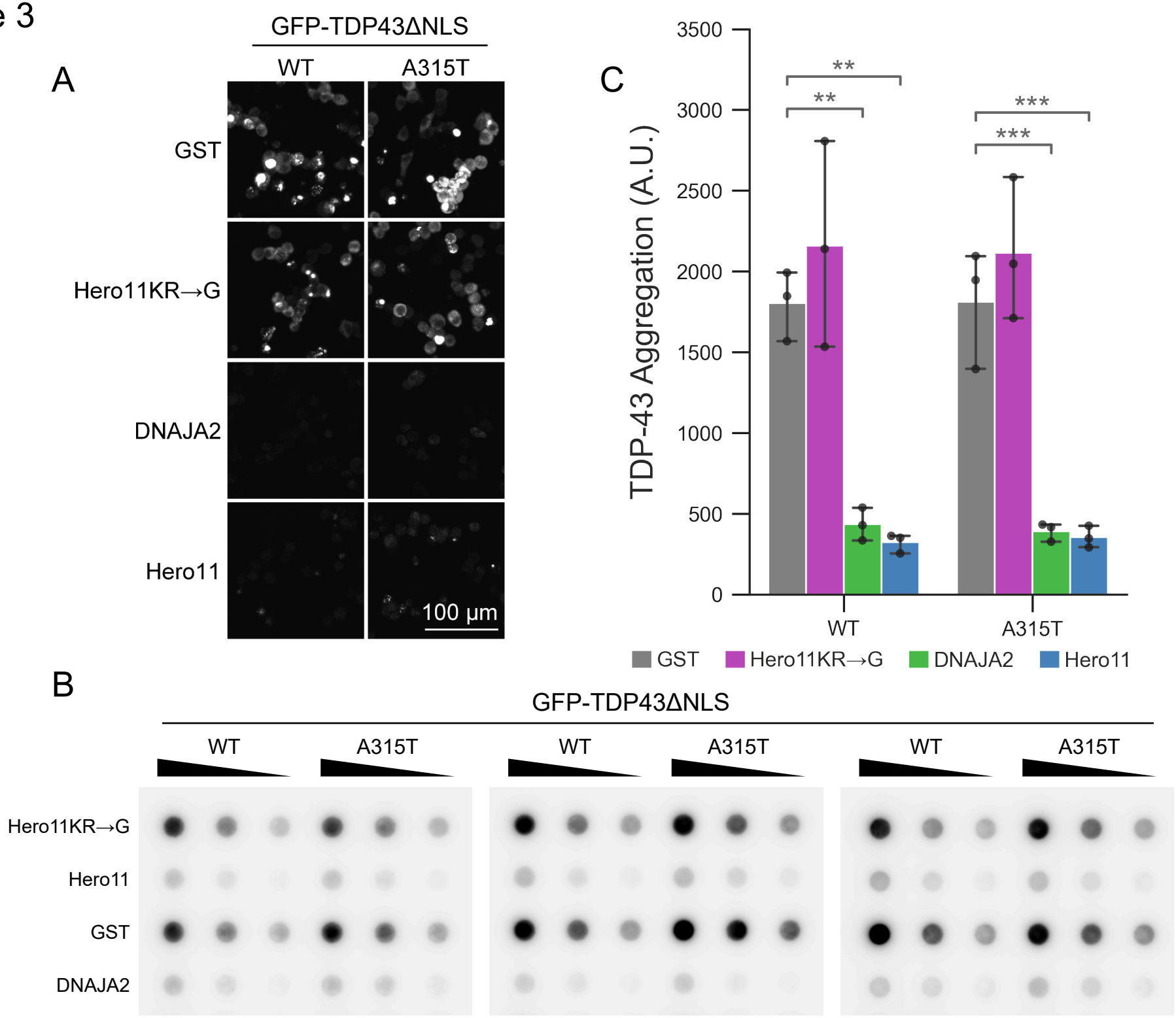
A
GFP-TDP43ΔNLS
WT
A315T
GST
Hero11KR→G
DNAJA2
Hero11
100 µm
C
TDP-43 Aggregation (A.U.)
3500
3000
2500
2000
1500
1000
500
0
**
**
***
***
WT
A315T
GST
Hero11KR→G
DNAJA2
Hero11
B
GFP-TDP43ΔNLS
WT
A315T
WT
A315T
WT
A315T
Hero11KR→G
Hero11
GST
DNAJA2

Figure 4

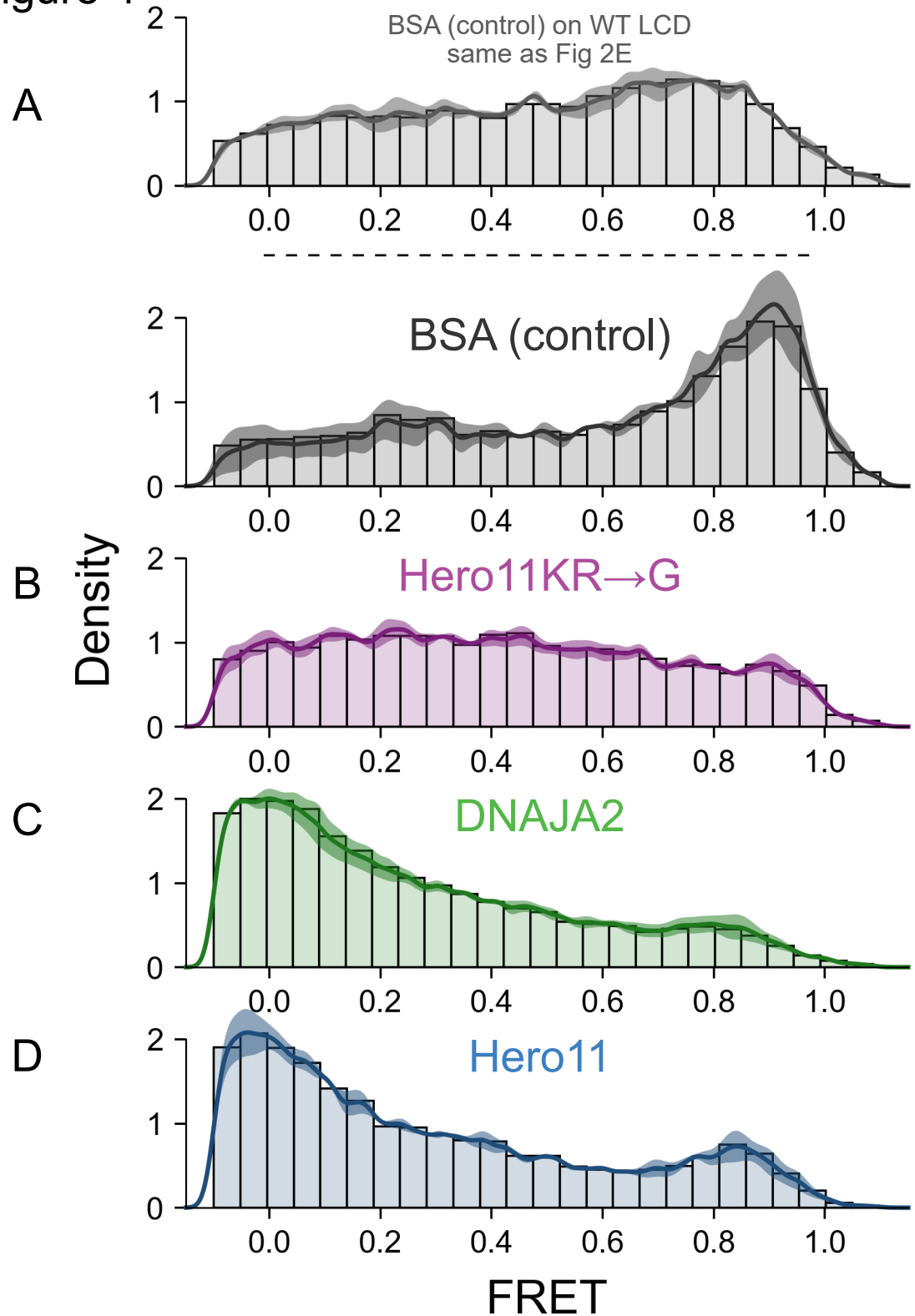
A
BSA (control) on WT LCD
same as Fig 2E
BSA (control)
B
Hero11KR→G
C
DNAJA2
D
Hero11
Density
FRET
0.0
0.2
0.4
0.6
0.8
1.0
0
1
2

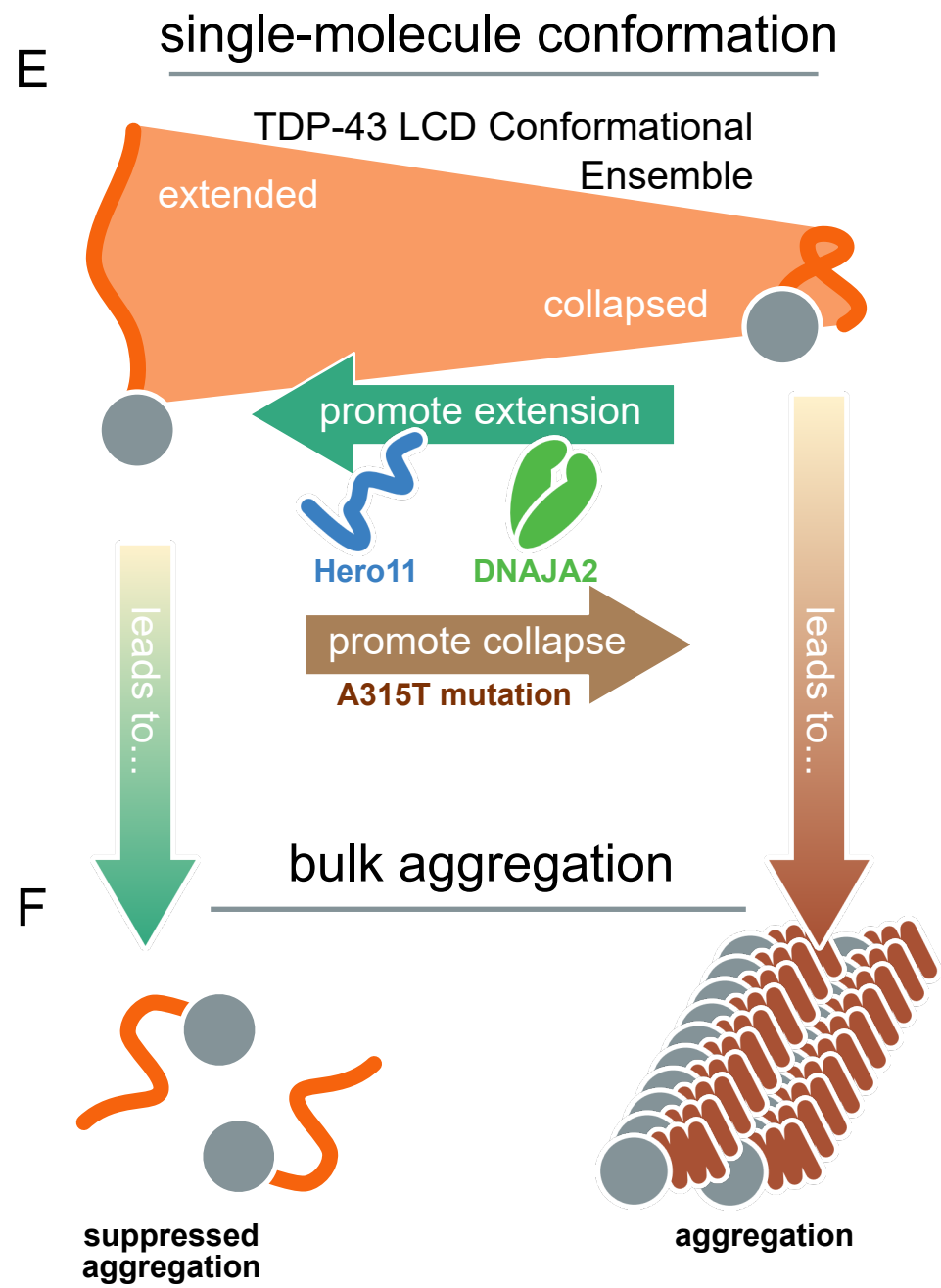
E
single-molecule conformation
TDP-43 LCD Conformational Ensemble
extended
collapsed
promote extension
Hero11
DNAJA2
promote collapse
A315T mutation
leads to...
leads to...
F
bulk aggregation
suppressed aggregation
aggregation

Supplementary Figure 1

A

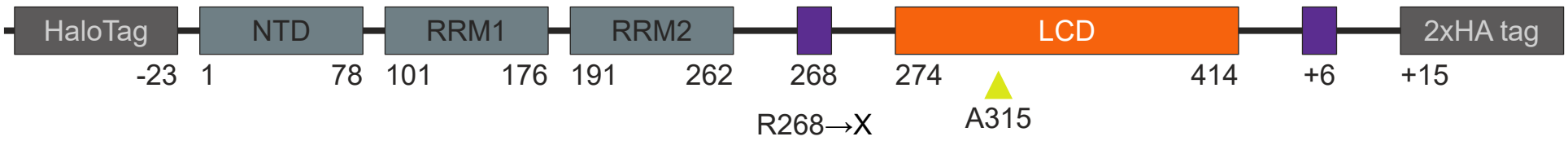


B

```
GMAEIGTGFPFDPHYVEVLGERMHYVDVGPRDGTPVLFLHG
NPTSSYVWRNIIPHVAPTHRCIAPDLIGMGKSDKPDLGYFF
DDHVRFMDAFIEALGLEEVVLVIHDWGSALGFHWAKRNPER
VKGIAFMEFIRPIPTWDEWPEFARETFQAFRTTDVGRKLII
DQNVFIEGTLPMGVVRPLTEVEMDHYREPFLNPVDREPLWR
FPNELPIAGEPANIVALVEEYMDWLHQSPVPKLLFWGTPGV
LIPPAEAARLAKSLPNCKAVDIGPGLNLLQEDNPDLIGSEI
ARWLSTLEISGHRYTSLYKKAGSAAELGTLEMSEYIRVTED
ENDEPIEIPSEDDGTVLLSTVTAQFPGACGLRYRNPVSQCM
RGVRLVEGILHAPDAGWGNLVYVVNYPKDNKRKMDETDASS
AVKVKRAVQKTSDLIVLGLPWKTTEQDLKEYFSTFGEVLMV
QVKKDLKTGHSKGFGFVRFTEYETQVKVMSQRHMIDGRWCD
CKLPNSKQSQDEPLRSRKVFVGRCTEDMTEDELREFFSQYG
DVMDVFIPKPFRAFAFVTFADDQIAQSLCGEDLIIKGISVH
ISNAEPKHNSNXQLERSGRFGGNPGGFGNQGGFGNSRGGGA
GLGNNQGSNMGGGMNFGAFSINPAMMAAAQAALQSSWGMMG
MLASQQNQSGPSGNNQNQGNMQREPNQAFGSGNNSYSGSNS
GAAIGWGSASNAGSGSGFNGGFGSSMDSKSSGWGMLEGSEX
KLVDLQSRYPYDVPDYASRYPYDVPDYASR*
```

768 amino acids
~85 kDa
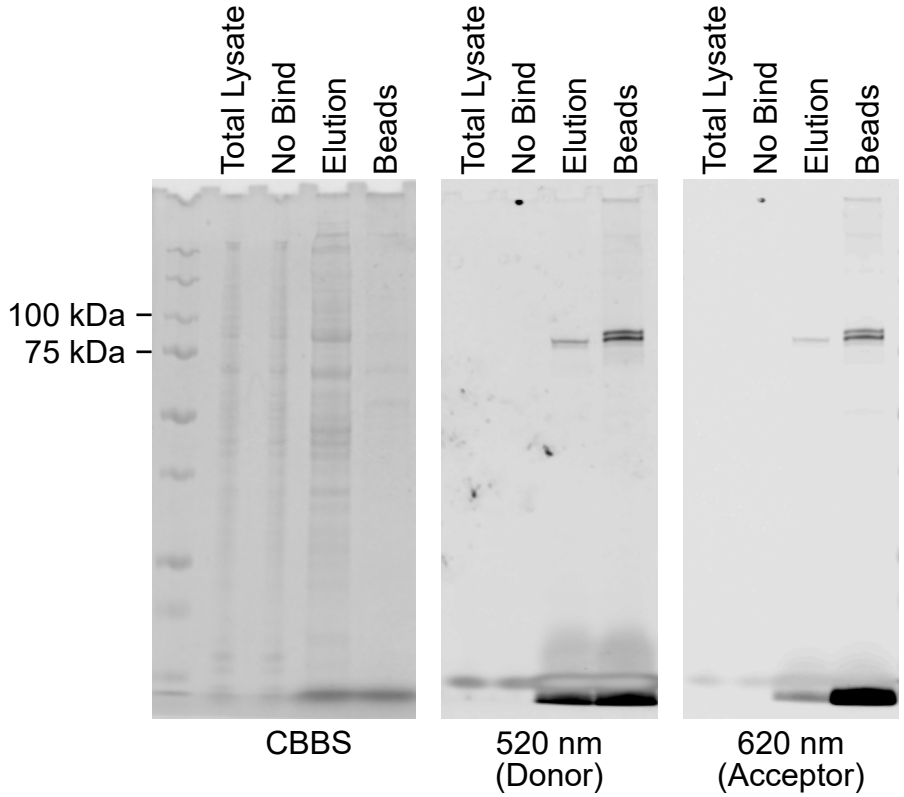
C